PCCP

PAPER

View Article Online
View Journal | View Issue

Cite this: *Phys. Chem. Chem. Phys.*, 2018, **20**, 6606

Computational identification of the binding mechanism of a triple reuptake inhibitor amitifadine for the treatment of major depressive disorder†

Weiwei Xue,[ab] Panpan Wang,[ab] Gao Tu,[ab] Fengyuan Yang,[ab] Guoxun Zheng,[ab] Xiaofeng Li,[ab] Xiaoxu Li,[ab] Yuzong Chen,[c] Xiaojun Yao[d] and Feng Zhu *[ab]

Amitifadine, the only drug ever clinically tested in Phase 3 for treating depression, is a triple reuptake inhibitor (TRI) that simultaneously interacts with human monoamine transporters (MATs) including hSERT, hNET and hDAT. This novel multi-target strategy improves drug efficacy and reduces the toxic side effects of drugs. However, the binding modes accounting for amitifadine's polypharmacological mode of action are still elusive, and extensive exploration of the amitifadine–target interactions between amitifadine and MATs is urgently needed. In this study, a total of 0.63 μs molecular dynamics (MD) simulations with an explicit solvent as well as endpoint binding free energy (BFE) calculation were carried out. MD simulation results identified a shared binding mode involving eleven key residues at the S1 site of MATs for the binding of amitifadine, and the results of the BFE calculations were in good agreement with experimental reports. Moreover, by analyzing the per-residue energy contribution variation at the S1 site of three MATs and additional cross-mutagenesis simulations, the variation in the inhibition ratio of amitifadine between hSERT and two other MATs was discovered to mainly come from non-conserved residues (Y95, I172 and T439 in hNET and Y95, I172, A169 and T439 in hDAT). As the rational inhibition ratio of multi-target drugs among various therapeutic targets was found to be the key to their safety and tolerance, the findings of this study may further facilitate the rational design of more potent but less toxic multi-target antidepressant drugs.

Received 22nd November 2017,
Accepted 31st January 2018

DOI: 10.1039/c7cp07869b

rsc.li/pccp

Introduction

Major depressive disorder (MDD) has been estimated to be the second largest global health burden among all diseases by 2030,[1–3] which makes the discovery of new and efficacious antidepressants an urgent task.[4–6] The first-line medications currently prescribed for MDD patients include selective reuptake inhibitors of serotonin (SSRIs), norepinephrine (sNRIs) and reuptake inhibitors of both serotonin and norepinephrine (SNRIs).[7–9] However, these medications are less than ideal considering their low remission rate,[10,11] delayed onset of action,[12,13] partial or non-response[14,15] and associated side effects.[16,17] Clinical investigation has revealed that that detuning of the triangular relationship among serotonin (5-HT), norepinephrine (NE) and dopamine (DA) drives the development of depression.[18] The increase of dopaminergic neurotransmission can alleviate the persistence of anhedonia (a core treatment-resistant symptom of MDD), and in turn gives rise to a rapid onset of action.[19,20] Therefore, an attractive strategy simultaneously inhibiting the reuptakes of 5-HT, NE and DA has been developed recently for MDD treatment,[16] and the resulting triple reuptake inhibitors (TRIs) are found to produce higher efficacy than first-line antidepressants.[21,22]

So far, a number of TRIs (listed in the ESI,† Table S1[16,23,24]) have advanced to clinical trial. Among these, amitifadine (also known as DOV-21,947 or EB-1010) is the only one which has ever been clinically tested in Phase 3 for treating depression.[16,24,25] Besides, this TRI and its analogues have also been investigated in clinical trials for treating other diseases including pain, alcohol use disorder, attention-deficit/hyperactivity disorder and smoking

[a] *Innovative Drug Research and Bioinformatics Group, College of Pharmaceutical Sciences, Zhejiang University, Hangzhou 310058, China*
[b] *Innovative Drug Research and Bioinformatics Group, School of Pharmaceutical Sciences and Collaborative Innovation Center for Brain Science, Chongqing University, Chongqing 401331, China*
[c] *Bioinformatics and Drug Design Group, Department of Pharmacy, National University of Singapore, Singapore 117543, Singapore*
[d] *State Key Laboratory of Applied Organic Chemistry and Department of Chemistry, Lanzhou University, Lanzhou 730000, China. E-mail: zhufeng.ns@gmail.com, zhufeng@zju.edu.cn*

† Electronic supplementary information (ESI) available. See DOI: 10.1039/c7cp07869b

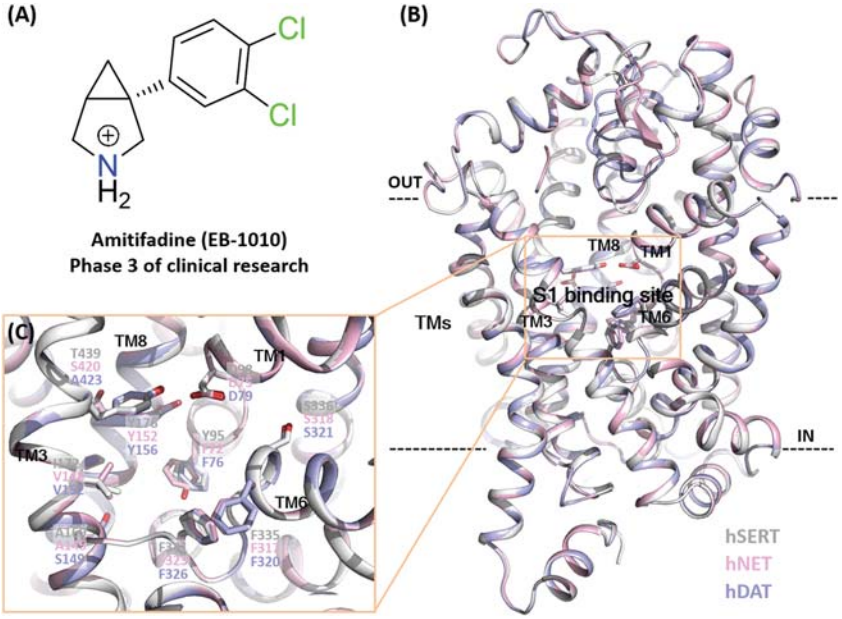

Fig. 1 (A) Structure of the triple reuptake inhibitor amitifadine. (B) Superimposition of the homology models of hSERT (gray), hNET (light pink) and hDAT (light blue) using the X-ray crystal structure of dDAT as the template. (C) Close view of the S1 binding site. The proteins are shown as cartoon. The S1 binding site residues are shown as sticks. The residues and TM regions are labeled as discussed in the text. The proteins were visualized using PyMOL.

cessation.[24–29] Amitifadine simultaneously inhibits the reuptake of 5-HT, NE and DA by multi-targeting human serotonin transporter (hSERT), norepinephrine transporter (hNET) and dopamine transporter (hDAT) with the binding affinities (measured by K_i values) of 99, 262 and 213 nM (Fig. 1A), respectively,[30] and its Phase 3 trial (ClinicalTrials.gov ID: NCT01318434) further suggests that the binding mode and the inhibition ratio on triple reuptakes are responsible for its improved drug safety and tolerance.[16,31]

For a long period of time, the understanding of drug-transporter interactions underlying the multi-target mechanism of amitifadine had been limited by a lack of knowledge of the 3D structure of monoamine transporters.[32–34] With the determination of crystal structures of bacterial LeuT[32] and *Drosophila melanogaster* dopamine transporter (dDAT),[33] molecular modelling based on these templates was applied to uncover the inhibitory mechanism of reuptake inhibitors,[35–42] and demonstrated great potential in predicting polypharmacology and facilitating multi-target drug design.[43–47] One particular example was that the binding mode of the SSRI antidepressant was successfully discovered in comparison to the newly determined X-ray structure of hSERT.[39,48,49] However, despite these great advances, the binding modes accounting for the polypharmacological mode of action of amitifadine are still elusive, and the extensive exploration of the TRI–target interactions between amitifadine and three monoamine transporters (MATs) is urgently needed.

Herein, an integrated computational strategy was used to discover the inhibitory mechanism of amitifadine on its three primary therapeutic targets (hSERT, hNET and hDAT) by revealing its binding mode at the atomic-level and quantitatively calculating its binding affinity. Firstly, the homology models of hSERT, hNET and hDAT were constructed using the crystal structure of dDAT as the template. Secondly, complexes of amitifadine bound to hSERT, hNET and hDAT were predicted by docking, and further assessed by molecular dynamics (MD) simulations with an explicit solvent and end-point binding free energy (BFE) calculations. The simulation model was validated by the co-crystal structure of dDAT in complex with 3,4-dichlorophenethylamine[50] and by a recently resolved crystal structure of hSERT.[48] Thirdly, the binding modes of amitifadine in those three targets were revealed and the results of BFE calculations were in good agreement with experiments.[30] Because the rational inhibition ratio of multi-target drugs among various therapeutic targets was found to be the key to their safety and tolerance, the inhibition ratio of amitifadine among three MATs was systematically explored by analyzing the energy variation of each residue at the S1 site of hSERT, hNET and hDAT and conducting *in silico* cross-mutagenesis studies. In summary, this study revealed the binding modes underlying amitifadine's polypharmacology, which drew a blueprint for assessing and discovering novel, safer and more effective TRIs for MDD treatment.

Materials and methods

System setup

Modelling of ligand–protein complexes and structural preparation. The 3D structure of amitifadine was taken from PubChem (CID: 11658655). The homology models of hSERT, hNET and hDAT were built using SWISS-MODEL[51] and a recently solved dDAT crystal structure (PDB: 4M48[33]) as the template. Sequence alignment for homology modelling was generated using ClustalW2.[52] The stereo-chemical quality of the models was further evaluated using PROCHECK[53] and no severe violation was identified in the Ramachandran plot.

Based on the align module of PyMOL,[54] two functional Na^+ ions in 4M48[33] were manually fitted into the S1 binding sites of hSERT, hNET and hDAT.

The Glide[55] docking method was used to get the initial structures of hSERT:amitifadine, hNET:amitifadine and hDAT:amitifadine. First, the structure of amitifadine was preprocessed using LigPrep[56] and the OPLS-2005 force field. The ionized state was assigned using Epik[57] at a pH value of 7.0 ± 2.0. The prepared amitifadine carried a net positive charge as shown in Fig. 1A. Then, hSERT, hNET and hDAT homology models were prepared by adding hydrogen atoms, assigning partial charges and protonation states, and minimizing the structures using the Protein Preparation Wizard module in Maestro.[58] Third, the residues (Tyr95, Asp98, Ile172, Asn177, Phe341 and Ser438 of hSERT, Phe72, Asp75, Val148, Gly149, Phe323 and Ser419 of hNET and Phe76, Asp79, Val152, Gly153, Phe326 and Ser422 of hDAT) identified as key determinants of the binding[59] of amitifadine were used to define the docking grid box. Docking was performed using standard precision (SP), and ligand sampling was set to flexible.

Protein–ligand/membrane–water complex. The complexes of amitifadine binding to hSERT, hNET and hDAT obtained by docking were pre-oriented in OPM[60] and then inserted into an explicit palmitoyl-oleoyl-phosphatidylcholine (POPC) lipid bilayer by means of the Membrane Builder module in CHARMM-GUI.[61] The TIP3P water[62] of 20 Å thickness was placed above and below the constructed bilayer. The systems were neutralized with Na^+ and Cl^- counterions at an environmental salt concentration of 0.15 M. The overall system contained ~96 000 atoms per periodic cell, and the box size was set as 83 Å × 83 Å × 127 Å.

MD simulation

All MD simulations were carried out using the GPU (NVIDIA Tesla K20C) accelerated PMEMD program in AMBER14.[63] The parameters of lipid (POPC) and transporter force fields were obtained from the AMBER ff14SB[62] and Lipid14.[64] The ion parameters of TIP3P water were collected from Joung & Cheatham.[65] The ligand (amitifadine) parameters were from the general AMBER force field (GAFF) with the charges derived from a RESP[66] fit using an HF/6-31G* electrostatic potential calculated using Gaussian09.[67]

In each simulation, the complex was minimized, heated and equilibrated as follows. The first step of energy minimization was to apply a harmonic restraint of 10 kcal mol^{-1} $Å^{-2}$ to the solute and lipid chains, and the second step was to allow all atoms to move freely. In each step, minimization was performed using the steepest descent method for the first 5000 steps and the conjugated gradient method for the subsequent 5000 steps. Following the minimization, the system was further heated through two sequential runs (100 ps) to 310 K in the *NVT* ensemble using a Langevin thermostat and with harmonic restraints of 10 kcal mol^{-1} $Å^{-2}$ on the lipid and solute atoms. Finally, unconstrained *NPT* dynamics (5 ns) at 310 K and 1 atm was carried out 10 times to equilibrate the system. The production simulation was conducted for 150 ns duration in the *NPT* ensemble at 310 K and 1 atm using periodic boundary conditions. Long-range electrostatic interactions (cutoff = 10 Å) were calculated using the Particle Mesh Ewald algorithm.[68] The integration time step was set to 2 fs and all hydrogen atoms were constrained using the SHAKE algorithm.[69]

Binding free energy calculation and per-residue energy decomposition analysis

The binding free energy (ΔG_{calc}) of amitifadine binding to hSERT, hNET and hDAT was obtained using the end-point molecular mechanics generalized Born surface area (MM/GBSA) and molecular mechanics Poisson–Boltzmann surface area (MM/PBSA) approach,[70–72] which is based on the following equation:

$$\Delta G_{calc} = \Delta E_{vdW} + \Delta E_{ele} + \Delta G_{pol} + \Delta G_{nonpol} \quad (1)$$

where ΔE_{vdW} and ΔE_{ele} indicate the van der Waals and electrostatic components in the gas phase, and ΔG_{pol} and ΔG_{nonpol} are the polar and non-polar solvent interaction energies. ΔE_{vdW} and ΔE_{ele} are calculated using the AMBER force field ff14SB,[62] and the electrostatic free energy of solvation (ΔG_{pol}) is calculated by solving the PB[73] or GB[74] equations. Solute and solvent dielectric constants were set to 2 and 80 similar to previous work.[39,40] ΔG_{nonpol} was calculated by $\Delta G_{nonpol} = 0.0072 \times \Delta SASA$,[75,76] where SASA is referred to the solvent accessible area. To evaluate the contribution of per-residue energy ($\Delta G_{calc}^{per\text{-}residue}$) to the binding of amitifadine, the total binding free energy could be decomposed by

$$\Delta G_{calc}^{per\text{-}residue} = \Delta E_{vdW}^{per\text{-}residue} + \Delta E_{ele}^{per\text{-}residue} + \Delta G_{pol}^{per\text{-}residue} + \Delta G_{nonpol}^{per\text{-}residue} \quad (2)$$

Each term in eqn (2) is defined in a similar way to that in eqn (1), except for the non-polar solvent interaction energy ($\Delta G_{nonpol}^{per\text{-}residue}$) calculated by recursive approximation of a sphere around an atom, starting from an ICOSA.

Hierarchical clustering analysis

The energy contributions of certain residues to the binding of amitifadine calculated in the previous section were used to generate a three-dimensional vector. Then, the per-residue energy contribution vector-based hierarchical tree of 237 residues with a contribution to amitifadine's binding to at least one transporter (contribution ≠ 0 kcal mol^{-1}) was generated using R analysis software[77] with the similarity levels among vectors measured by the Manhattan distance:

$$\text{Distance } (a,b) = \sum_i |a_i - b_i| \quad (3)$$

where i denotes each dimension of per-residue energies a and b. The cluster algorithm used here is the Ward's minimum variance method,[78] which was designed to minimize the total within-cluster variance. The Ward's minimum variance module in R analysis software[77] was used, and the hierarchical clustering tree graph was generated using the online tree generator iTOL.[79]

Results and discussion

Constructing the homology models of hSERT, hNET and hDAT

To understand the inhibitory mechanism of amitifadine, the structural information of three MATs is indispensable. Herein, the 3D structures of three MATs (Fig. 1B, hSERT from Glu78 to Pro617, hNET from Gln54 to Glu597, hDAT from Gln58 to Asp600) were constructed by homology modelling based on the X-ray crystal structure (PDB code: 4M48[33]) of dDAT (from Glu26 to Asp599). All structures covered 12 transmembrane (TM) regions and the corresponding intervening loops (Fig. 1B). The stereo chemical quality and accuracy of the predicted model were evaluated using PROCHECK.[53] Ramachandran plots showed 99.6%, 99.8% and 99.8% of the residues in the modeled hSERT, hNET and hDAT located in the "allowed region" (ESI,† Fig. S2), indicating a high quality of the overall main chain and side chain conformations. In addition, the crystal structure of hSERT (PDB code 5I6Z[48]) was released very recently, and a comparison of the hSERT homology model with the solved X-ray crystal structure was conducted. As expected, the homology model of hSERT was highly consistent with the crystal structure (ESI,† Fig. S3), which was provided as one line of evidence validating the model constructed (see the "Validation of the molecular models" section).

Predicting and assessing the initial structures of amitifadine–MAT complexes

To obtain the initial structures of protein–ligand complexes, amitifadine was docked into the S1 binding site of the modelled hSERT, hNET and hDAT (primarily surrounded by TM1, TM3, TM6, and TM8 regions) using Glide SP docking.[43] In previous studies,[39,40,48,80] the docking procedure was successfully used to predict the binding mode of antidepressants in hSERT and hNET. Herein, the docking poses of amitifadine similar to the orientation of sertraline co-crystallized with dDAT[81] were selected for subsequent MD simulations. All binding poses of amitifadine selected in this work included the salt bridge and hydrophobic interaction with the S1 binding sites of MATs (ESI,† Fig. S4).

Based on the initial amitifadine–MAT complexes constructed by docking, MD simulations were conducted to incorporate conformational flexibility into both MATs and the ligand and to assess the persistence of the key interactions. As a result, the monitored root mean square deviation (RMSD) of 3 MATs as well as the ligand binding site (residues within 5 Å of the bound amitifadine) backbone atoms and ligand heavy atoms showed that the RMSDs reached equilibration within 150 ns simulation for each complex (ESI,† Fig. S5). Structural superimposition of the docking pose and an MD representative snapshot of amitifadine at the binding sites of MATs indicated sight conformation shifts (the RMSDs of amitifadine in hSERT, hNET and hDAT before and after MD simulations were 0.82 Å, 1.17 Å and 1.37 Å, respectively), but the key interactions such as the salt bridge between the protonated nitrogen of ligands and the conserved aspartate of proteins (Asp98 in hSERT, Asp75 in hNET and Asp79 in hDAT) were preserved (ESI,† Fig. S6). Thus, the last 50 ns equilibrated simulation trajectories were adopted to further estimate the molecular basis of amitifadine's binding specificity to hSERT, hNET and hDAT.

Estimating the binding affinity of amitifadine to MATs

The binding free energy (ΔG_{calc}) of amitifadine to each MAT was estimated using the last 50 ns equilibrated simulation trajectories using MM/GB(PB)SA methods.[70,71,73] Compared with the absolute binding free energy assessed using the alchemical method,[82,83] this kind of end-point calculation was more computationally efficient to obtain the relative order of ligands binding to proteins of one single family.[81,84–86] Meanwhile, this has been used to explain the multitarget drug binding.[87–90] In this study, the ΔG_{calc} values of amitifadine using MM/GB(PB)SA methods are equal to −40.65 (−46.97), −38.50 (−46.10) and −38.59 (−44.15) kcal mol^{-1} for hSERT, hNET and hDAT (Table 1), respectively. In addition, the experimental binding affinities (ΔG_{exp}) were estimated based on the K_i values[30] using $\Delta G_{exp} = RT\ln(K_i)$. As shown in Table 1, despite the overestimation of binding affinity using MM/GB(PB)SA methods,[91–94] $\Delta\Delta G_{calc,GB}$ was able to capture the relative order of $\Delta\Delta G_{exp}$. The calculated values of the relative binding free energy ($\Delta\Delta G_{calc,GB}$) were in good accordance with those of experimental results ($\Delta\Delta G_{exp}$) with a high correlation coefficient (R^2) of 0.93, while the correlation coefficient between $\Delta\Delta G_{calc,PB}$ and $\Delta\Delta G_{exp}$ was only 0.33. Moreover, additional three short simulations (50 ns) for each system starting from the equilibrated trajectories (ESI,† Fig. S7) were conducted to confirm the obtained binding free energies (ESI,† Table S2). The mean values of correlation coefficients between ΔG_{calc} and ΔG_{exp} were 0.99 and 0.96 for GB and PB calculations, respectively. The results indicated that GB calculations were more suitable to obtain the relative order of amitifadine binding to three MATs. The detailed information of the calculated contribution of each energy term in eqn (1) revealed that the binding of amitifadine to hSERT, hNET and hDAT was primarily driven by van der Waals (ΔE_{vdW}) and electrostatic interaction energies (ΔE_{ele}), but is hampered by polar solvent energies (ΔG_{pol}), as summarized in the ESI,† Table S2.

Table 1 The calculated and experimental binding free energies of the studied TRI binding to hSERT, hNET and hDAT (ΔG is in kcal mol^{-1} and K_i value is in nM)

TRI	Targets	$\Delta G_{calc,PB}$[a]	$\Delta\Delta G_{calc,PB}$[b]	$\Delta G_{calc,GB}$[a]	$\Delta\Delta G_{calc,GB}$[b]	ΔG_{exp}[c]	$\Delta\Delta G_{exp}$[b]	K_i[d]
Amitifadine	hSERT	−46.97	0	−40.65	0.00	−9.55	0.00	99.00
	hNET	−46.10	0.87	−38.50	2.15	−8.97	0.58	262.00
	hDAT	−44.15	2.82	−38.59	2.06	−9.10	0.45	213.00

[a] Calculated binding energy using MM/GB(PB)SA method in this work. [b] Binding free energy variation was calculated using the amitifadine–hSERT complex as a reference. [c] Estimated binding free energy based on K_i values using $\Delta G_{exp} = RT\ln(K_i)$. [d] Experimental K_i value from the previous study.[30]

Validation of the constructed molecular models

Besides the good accordance between the calculated and experimental relative binding free energies in the previous section, two lines of additional evidence were provided to validate the simulation models.

First: structural comparison with 3,4-dichlorophenethylamine in complex with dDAT. As illustrated in Fig. S8A (ESI†), amitifadine and 3,4-dichlorophenethylamine shared great structural similarity with a high tanimoto coefficient value (0.85).[95] Due to the absence of the co-crystal structure of amitifadine, the structure of dDAT in complex with 3,4-dichlorophenethylamine (PDB code 4XPA[50]) provided valuable information for validating the models constructed in this study. The crystallographic study showed that 3,4-dichlorophenethylamine fitted into the S1 binding pocket of dDAT[50] with the amine group forming hydrogen bonds with the carboxyl group of Asp46 and the carbonyl group of Phe319 and the dichlorophenyl ring bordered using Val120 and Phe325. Herein, the molecular model in Fig. 2(A2, B2 and C2) shows that the protonated nitrogen of amitifadine interacts with the carboxylate of the conserved aspartate in three MATs (Asp98 in hSERT, Asp75 in hNET, and Asp79 in hDAT), and the dichlorophenyl ring of amitifadine is also contacted with the corresponding two hydrophobic residues (Ile172 and Phe341 in hSERT, Val148 and Phe323 in hNET, and Val152 and Phe326 in hDAT). Superimposition of the representative snapshots of amitifadine bound in three MATs onto the co-crystal structure 4XPA of dDAT further revealed strikingly similar features between amitifadine and 3,4-dichlorophenethylamine (Fig. S8(B–D), ESI†).

Second: successful reproduction of the crystal structure of hSERT. The very recently determined X-ray crystal structure of hSERT[48] also provided valuable data for validating the simulation models. As shown in the ESI,† Fig. S3A and Table S3, the homology models of hSERT generated in this study were in considerable accordance with the determined hSERT crystal structure (RMSDs of the whole structure and transmembrane domain are equal to 2.45 Å and 1.33 Å, respectively). In particular, the overlay between the constructed hSERT model and its crystal structure showed strong similarity at the S1 binding site (RMSD is equal to 0.80 Å) primarily surrounded by the TM1, TM3, TM6, TM8 and TM10 regions (ESI,† Fig. S3B). These data demonstrated that the hSERT models generated based on the crystal structure of dDAT could serve as an effective platform for exploring antidepressant binding at theS1 binding site of hSERT. Moreover, MD simulation and binding free energy estimation of the co-crystal structure of hSERT in complex with escitalopram (an approved SSRI for treating MDD) were carried out.[80] Simulation results revealed a consistent structural feature (RMSDs of the whole structure, the S1 binding site

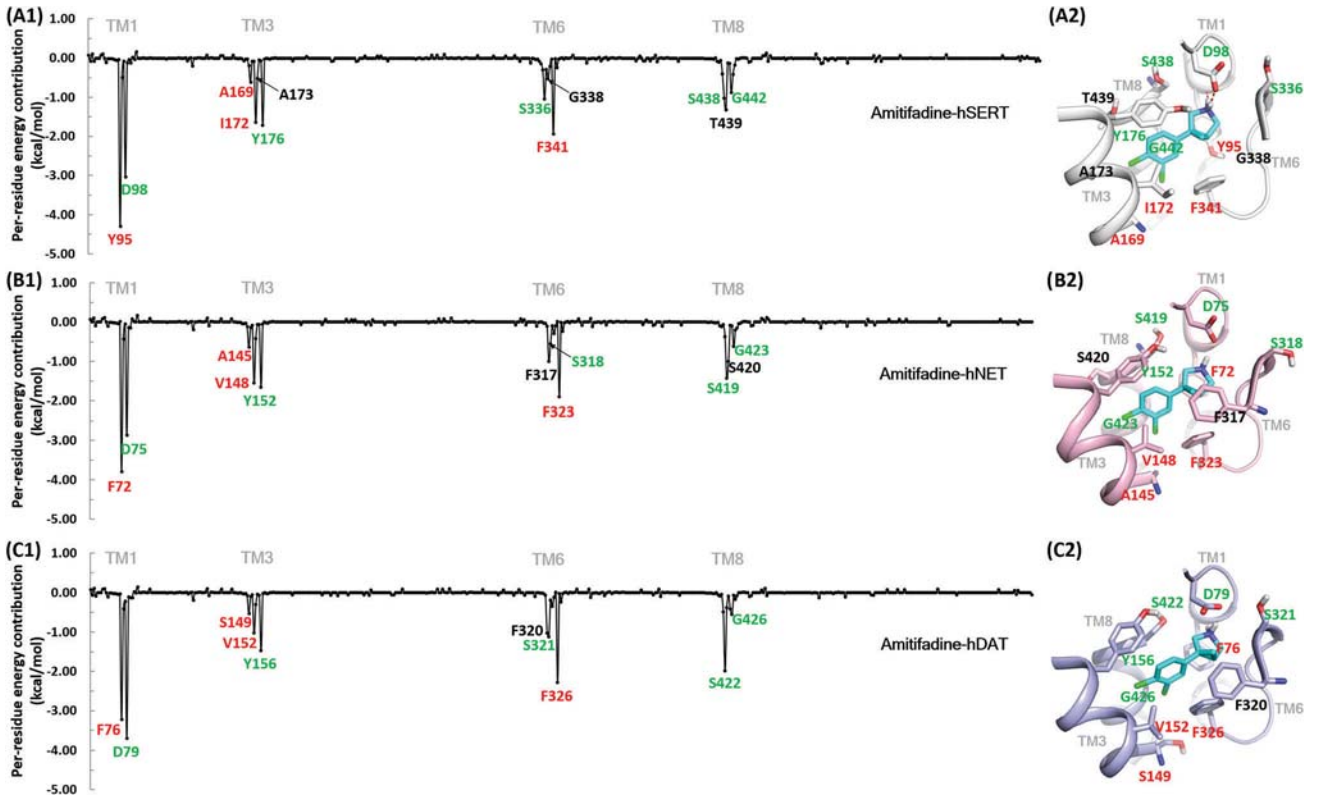

Fig. 2 (A1–C1) Per-residue contributions (MM/GBSA) of binding energies of the three studied protein–ligand complexes. (A2–C2) Proposed binding modes of amitifadine (cyan) at the S1 binding site of hSERT (gray), hNET (light pink) and hDAT (light blue). Cartoon representation was used for the protein. The residues and ligands are shown in stick representation, and only polar hydrogen atoms are displayed for clarity. To get a better view, the residues only in proximity of the binding sites (TM1, 3, 6 and 8) having an important role in ligand binding are shown. The protein–ligand complexes were visualized using PyMOL.

and the ligand were 3.13 Å, 1.01 Å and 1.23 Å, respectively) and stable binding free energies (RMSE is equal to 0.20 kcal mol^{-1}) for drug binding as reported in the previous study.[39] Therefore, the computational method applied in this study was effective in identifying the pharmacology of human MATs based on the template of dDAT.[80]

Analyzing the binding mode of amitifadine–MAT complexes based on per-residue energy decomposition

To determine the key molecular determinants in three MATs responsible for the binding of amitifadine. The MM/GBSA and MM/GBSA per-residue based energy decomposition of the interaction energy in each complex was applied in this study and is shown in Fig. 2 and ESI,† Fig. S9, respectively. As illustrated in Fig. 2, the residues in four transmembrane regions (TM1, TM3, TM6 and TM8) mainly contributed to the binding of amitifadine (ESI,† Table S4 provided detailed information of the per-residue energy contribution). To the best of our knowledge, Fig. 2 provided the first panorama describing the binding energy of a TRI at the per-residue basis. In total, 12, 11 and 10 residues were identified as a high contribution one ($|\text{contribution}| \geq 0.5$ kcal mol^{-1} to the binding of amitifadine) in hSERT, hNET and hDAT, respectively. As shown in Fig. 2, the energy contribution of the corresponding residue among three MATs vary greatly (for example, the corresponding residues Tyr95 in hSERT, Phe72 in hNET and Asp79 in hDAT contributed -4.30 kcal mol^{-1}, -3.79 kcal mol^{-1} and -3.69 kcal mol^{-1}, respectively), to the binding of amitifadine. Fig. 2 also inferred a certain level of similarity among the studied three complexes, which inspired us to conduct further identification of the common features shared by hSERT, hNET and hDAT facilitating the binding of amitifadine. However, compared with MM/GBSA results, the MM/PBSA per-residue contribution cannot well reflect and distinguish the real interaction energy between amitifadine and S1 pocket residues in MATs (ESI,† Table S4). And ESI,† Fig. S9 demonstrated that the PB values overestimated the energy contributions from residues with negative charge such as Asp (D) and Asn (E). Therefore, the per-residue energy contributions from MM/GBSA calculations were used for further analysis.

Common features shared by three MATs facilitating the binding of amitifadine

The common features shared by multiple therapeutic targets of a specific drug can facilitate the design and discovery of novel one-probe multi-target lead scaffolds.[96] In this study, the

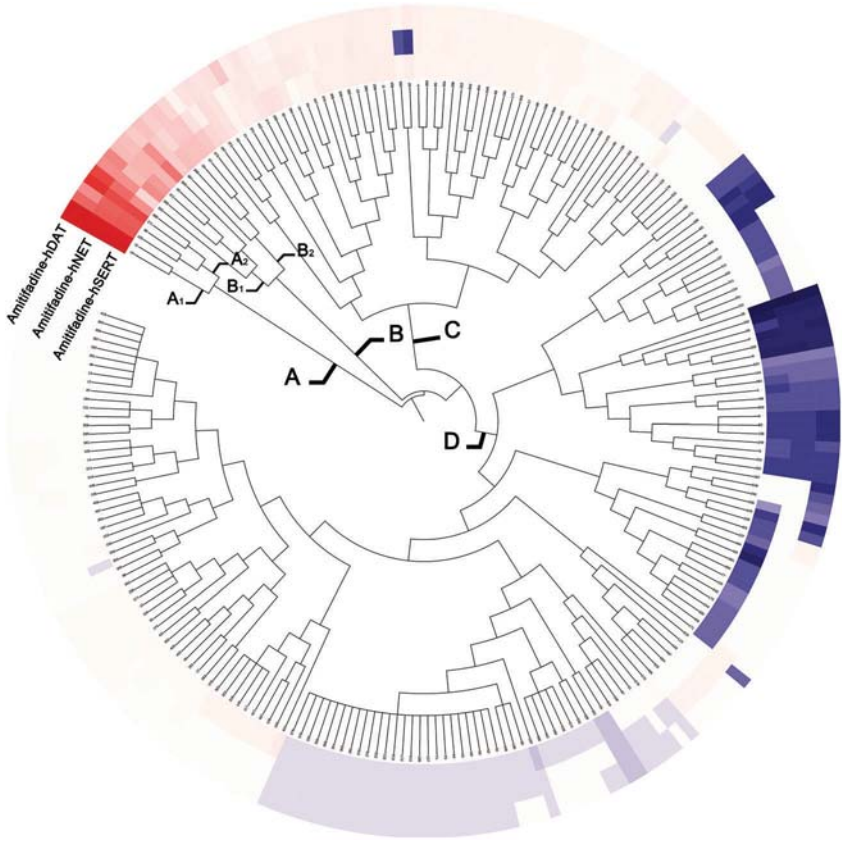

Fig. 3 Hierarchical clustering tree of residues contribute to amitifadine binding by their per-residue energy. Binding energy contributions favoring amitifadine binding are displayed in red, with the highest contribution (-4.30 kcal mol^{-1}) set as exact red and lower contributions gradually fading towards white (contribution is equal to 0 kcal mol^{-1}). Meanwhile, binding energy contributions hampering amitifadine binding are shown in blue, with the highest one (0.17 kcal mol^{-1}) set as exact blue and lower ones gradually fading towards white. It is necessary to clarify that the absolute value of the highest contribution favoring the binding of amitifadine (exact red) is 25 times higher than that hampering the binding (exact blue).

hierarchical clustering analysis of per-residue binding free energies was performed to identify the common features shared by three MATs facilitating the binding of amitifadine. As illustrated in Fig. 3, four distinct residue groups (A, B, C and D) were identified. It was clear that the energy contributions of residues in group A (Tyr95, Asp98, Ile172, Tyr176, Phe341 and Ser438 in hSERT, Phe72, Asp75, Val148, Tyr152, Phe323 and Ser419 in hNET, and Phe76, Asp79, Val152, Tyr156, Phe326 and Ser422 in hDAT) were consistently higher than those of groups B, C and D. Thus, the energy contribution of residues in group A composed the primary portion of the total energy contribution (59.74%, 62.77% and 61.87% for hSERT, hNET and hDAT, respectively). In addition, the energy contribution of residues in subgroup B_1 (Ala169, Phe335, Ser336, Thr439 and Gly442 in hSERT, Ala145, Phe317, Ser318, Ser420, Gly423 in hNET, and Ser149, Phe320, Ser321, Ala423, Gly426 in hDAT) was 18.03%, 17.97% and 16.26% of the total free energy for hSERT, hNET and hDAT, respectively. In this study, the residues in group A and subgroup B_1 were thus identified as the hot spots with "strong" or "relatively strong" contributions to the binding of amitifadine. As a result, 11 corresponding residues were identified as common features shared by three MATs facilitating the binding of amitifadine.

These common features could be further generalized and schematically represented in Fig. 4. As shown, a shared binding mode was defined by the collective electrostatic and hydrophobic interactions between 11 hot spots and amitifadine. Residues with "strong" and "relatively strong" contribution are colored in black and gray, respectively. The protonated nitrogen atom formed electrostatic interactions with Asp98 in hSERT, Asp75 in hNET and Asp79 in hDAT, and the dichlorophenyl ring mainly formed hydrophobic interactions with Tyr95, Ala169, Ile172, Tyr176, Ser438, Thr439 and Gly442 in hSERT, Phe72, Ala145, Val148, Tyr152, Ser419, Ser420 and Gly423 in hNET, and Phe72, Ser149, Val152, Tyr156, Ser422, Ala423 and Gly426 in hDAT. Furthermore, the azabicyclo contacted with Phe335, Series36 and Phe341 in hSERT, Phe317 Ser318 and Phe323 in hNET and Phe320, Ser321 and Phe326 in hDAT.

Exploring the origins of the inhibition ratio of MATs by amitifadine

For multi-target drugs, especially TRIs, their rational inhibition ratio among various therapeutic targets was found to be the key to their safety and tolerance.[16] As reported, the ratio of a drug inhibiting different targets depended on its efficiency measured by variations in binding free energy.[31] Herein, the inhibition ratio of amitifadine among three MATs was systematically explored by analyzing energy variation of each residue at the S1 site of hSERT, hNET and hDAT and conducting *in silico* cross-mutagenesis studies.

Energy variation of individual residues at the S1 site of MATs. Fig. 5 illustrated the calculated variation of the energy contribution of residues to the binding of amitifadine at the S1 site of three MATs (detailed information is provided in the ESI,† Table S5). Moreover, the superimposition of the conformations of protein–ligand interaction was also provided. As illustrated, most residues at the S1 site offered a similar degree of contribution to the binding of amitifadine among three different MATs, which is in accordance with the common features identified in Fig. 4. However, the BFE contributions of several residues varied significantly between different MATs. In particular, Tyr95 and Ser336 in hSERT made more contributions to

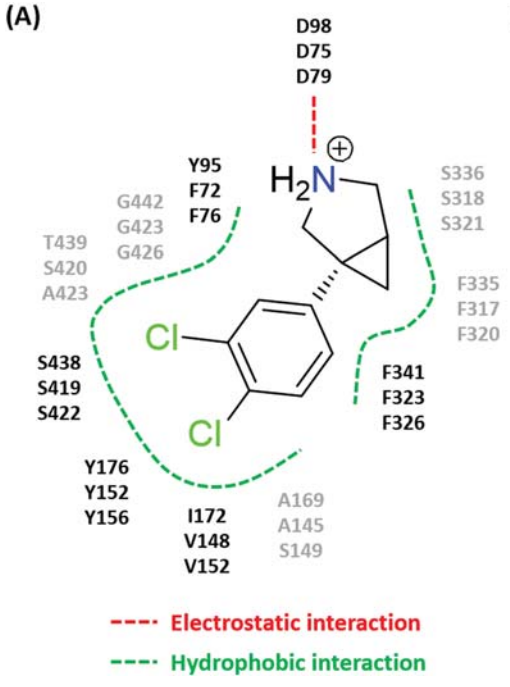

(B)

hSERT	hNET	hDAT
Y95	F72	F76
D98	D75	D79
I172	V148	V152
Y176	Y152	Y156
F341	F323	F326
S438	S419	S422
A169	A145	S149
F335	F317	F320
S336	S318	S321
T439	S420	A423
G442	G423	G426

Fig. 4 Schematic diagram of common interaction patterns of amitifadine with hSERT, hNET and hDAT. The identified electrostatic and hydrophobic interactions are depicted by red and light blue dashed lines, respectively.

the binding of amitifadine than the corresponding residues (Phe72 and Ser318) in hNET, while Phe317 and Ser419 in hNET contributed more BFE than the corresponding residues (Phe335 and Ser438) in hSERT (Fig. 5A1). Similar to the comparison between hSERT and hNET, the residues with a significant difference in BFE contribution between hSERT and hDAT (Fig. 5B1) included Tyr95, Phe335 and Ser438 in hSERT (Phe76, Phe320 and Ser422 in hDAT). In the meantime, Ile172 and Thr439 in hSERT made more contributions to the binding of amitifadine than the corresponding residues (Val152 and Ala423) in hDAT, while Asp79 in hDAT contributed more BFE than the corresponding residues (Asp98) in hSERT (Fig. 5B1). In addition, Fig. 5C1 revealed that Asp75, Ser318 and Ser419 in hNET made more contributions than the corresponding residues Asp79, Ser321 and Ser422 in hDAT, while residues Phe72, Val418 and Ser420 in hNET make less contributions than the corresponding residues (Phe76, Val152 and Ser423) in hDAT. The superposed conformations of protein–ligand interactions showed that energy contribution variation originated from the structural rearrangements of the corresponding residues when amitifadine accommodated into different pockets (Fig. A2, B2 and C2). As a result, the identified residues play a significant role in distinguishing binding free energy of amitifadine binding to hSERT, hNET and hDAT.

***In silico* cross-mutagenesis studies.** As reported, the non-conserved mutations at S1 sites among three MATs may contribute to the higher affinity of amitifadine binding to hSERT compared with that to hNET and hDAT.[16] It is of great interest to further evaluate the contribution of those non-conserved residues identified in the previous section. In this work, mutations at the S1 site of hSERT were thus conducted to transfer hNET-like or hDAT-like pharmacology to hSERT (Table 2). The initial structure of these mutated complexes were derived from the assessed wild type amitifadine–hSERT model and additional 20 ns MD simulations were carried out. The calculated BFEs ranged from −37.46 to −38.87 kcal mol^{-1} (Table 2, detailed energy terms could be found in the ESI,† Table S4). Compared to the wild type amitifadine-hSERT (−40.65 kcal mol^{-1}), the transfer of hNET-like or hDAT-like pharmacology to hSERT resulted in significant shifts in the BFEs (2.93 kcal mol^{-1} for hNET-like Y95F-I172V-T439S mutant and 3.14 kcal mol^{-1} for hDAT-like Y95F-I172V-A169S-T439S mutant), which substantially recovered the pharmacology of hNET and hDAT. As shown in Table 2, mutagenesis studies on single mutation could also result in shifts of the BFEs, but the corresponding effects were less significant than those of the multiple mutations (hNET-like Y95F-I172V-T439S and hDAT-like Y95F-I172V-A169S-T439S). Overall, the pharmacology of hNET or hDAT was largely recovered by mutations on those non-conserved residues identified in the previous section at the S1 site of hSERT, which reflected the key role of

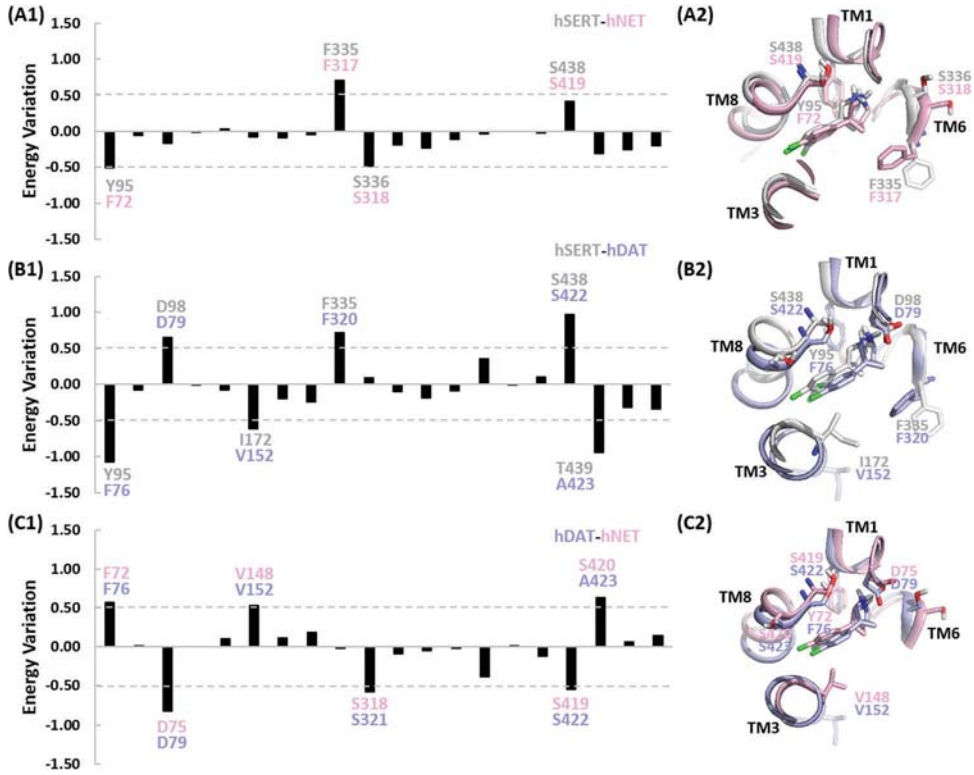

Fig. 5 (A1–C1) Plots of the fold change of the residue energy contribution levels of the residue at the S1 binding site between hSERT and hNET, hSERT and hDAT, and hNET and hDAT. (A2–C2) Comparison of the triple reuptake inhibitor amitifadine conformations by MD simulations at the S1 binding site of hSERT (gray), hNET (light pink) and hDAT (light blue). The ligand and binding site residues are shown as sticks. The proteins are shown as cartoon. The residues and TM regions are labeled as discussed in the text. 2D structure of the ligand are depicted in Fig. 1A. The protein–ligand complexes are visualized using PyMOL.

Table 2 The calculated binding energy changes of amitifadine–hSERT complexes before and after hNET-like or hDAT-like hSERT by *in silico* single and multiple mutagenesis studies (ΔG is in kcal mol^{-1})

		Calculated value		Experimental value
Targets	Mutations	ΔG_{calc}	$\Delta\Delta G_{calc}$ [a]	$\Delta\Delta G_{exp}$ [b]
hNET-like	Y95F	−38.87	1.78	2.15
	I172V	−38.30	2.35	
	T439S	−38.64	2.01	
	Y95F-I172V-T439S	−37.72	2.93	
hDAT-like	Y95F	−38.87	1.78	2.06
	A169S	−38.46	2.19	
	I172V	−38.30	2.35	
	T439A	−38.35	2.30	
	Y95F-I172V-A169S-T439S	−37.51	3.14	

[a] $\Delta\Delta G_{cal} = \Delta G_{mutation} - \Delta G_{wild\ type}$ (the $\Delta G_{wild\ type}$ value of the amitifadine–hSERT complex is listed in Table 2 and the ESI, Table S2). [b] $\Delta\Delta G_{exp}$ values were derived from the FC_{exp} by the equation $\Delta\Delta G_{exp} = RT\ln(FC_{exp})$, $FC_{exp} = K_i(hNET)/K_i(hSERT)$ or $K_i(hDAT)/K_i(hSERT)$ in ref. 30.

those mutations in affecting the various inhibition ratios of amitifadine among three MATs.

Conclusion

In this study, MD simulations, BFE calculations and per-residue energy decomposition analyses were carried out for a triple reuptake inhibitor, amitifadine (the only drug ever clinically tested in Phase 3 for treating depression), in complex with hSERT, hNET and hDAT. Our primary goal was to predict the binding mode at the atomic-level and obtain quantitative information of binding affinities. The calculated BFE follows consistently the order of the experimental results. By quantitatively analyzing the amitifadine–MAT interaction mode, the common features for amitifadine binding to MATs were identified. In addition, the energy variation analysis of the residues at the S1 site of hSERT, hNET and hDAT contributes to the binding of amitifadine and *in silico* cross-mutagenesis studies discovered that its variation in the inhibition ratio between hSERT and two other MATs (hNET and hDAT) mainly comes from the non-conserved residues (Y95F-I172V-T439S in hNET and Y95F-I172V-A169S-T439S in hDAT). In summary, for the first time, an accurate model of amitifadine–MAT interaction was generated, and provided significant insights into the origins of the hSERT, hNET and hDAT inhibition ratio by amitifadine. The results will facilitate rational optimization of multi-target antidepressants with improved pharmacological properties.

Conflicts of interest

There are no conflicts to declare.

Acknowledgements

This work was supported by the National Natural Science Foundation of China (21505009), Precision Medicine Project of the National Key Research and Development Plan of China (2016YFC0902200), Innovation Project on Industrial Generic Key Technologies of Chongqing (cstc2015zdcy-ztzx120003), Fundamental Research Funds for Central Universities (10611CDJXZ238826, CDJZR14468801, CDJKXB14011).

References

1 C. Global Burden of Disease Study, Lancet, 2015, **386**, 743–800.
2 G. Zheng, W. Xue, F. Yang, Y. Zhang, Y. Chen, X. Yao and F. Zhu, *Phys. Chem. Chem. Phys.*, 2017, **19**, 28885–28896.
3 P. Wang, X. Zhang, T. Fu, S. Li, B. Li, W. Xue, X. Yao, Y. Chen and F. Zhu, *ACS Chem. Neurosci.*, 2017, **8**, 1416–1428.
4 M. J. Ramaker and S. C. Dulawa, *Mol. Psychiatry*, 2017, **22**, 656–665.
5 F. Y. Yang, T. T. Fu, X. Y. Zhang, J. Hu, W. W. Xue, G. X. Zheng, B. Li, Y. H. Li, X. J. Yao and F. Zhu, *Mol. Simul.*, 2017, **43**, 1089–1098.
6 Y. H. Li, P. P. Wang, X. X. Li, C. Y. Yu, H. Yang, J. Zhou, W. W. Xue, J. Tan and F. Zhu, *PLoS One*, 2016, **11**, e0165737.
7 M. G. Caron and U. Gether, *Nature*, 2016, **532**, 320–321.
8 Y. H. Li, C. Y. Yu, X. X. Li, P. Zhang, J. Tang, Q. Yang, T. Fu, X. Zhang, X. Cui, G. Tu, Y. Zhang, S. Li, F. Yang, Q. Sun, C. Qin, X. Zeng, Z. Chen, Y. Z. Chen and F. Zhu, *Nucleic Acids Res.*, 2018, **46**, D1121–D1127.
9 F. Zhu, X. X. Li, S. Y. Yang and Y. Z. Chen, *Trends Pharmacol. Sci.*, DOI: 10.1016/j.tips.2017.12.002.
10 C. B. Nemeroff, R. Entsuah, I. Benattia, M. Demitrack, D. M. Sloan and M. E. Thase, *Biol. Psychiatry*, 2008, **63**, 424–434.
11 J. Xu, P. Wang, H. Yang, J. Zhou, Y. Li, X. Li, W. Xue, C. Yu, Y. Tian and F. Zhu, *BioMed Res. Int.*, 2016, 2509385.
12 F. Artigas, *ACS Chem. Neurosci.*, 2013, **4**, 5–8.
13 Y. H. Li, J. Y. Xu, L. Tao, X. F. Li, S. Li, X. Zeng, S. Y. Chen, P. Zhang, C. Qin, C. Zhang, Z. Chen, F. Zhu and Y. Z. Chen, *PLoS One*, 2016, **11**, e0155290.
14 G. I. Papakostas, *J. Clin. Psychiatry*, 2009, **70**, e18.
15 L. Tao, F. Zhu, F. Xu, Z. Chen, Y. Y. Jiang and Y. Z. Chen, *Pharmacol. Res.*, 2015, **102**, 123–131.
16 L. Shao, W. Li, Q. Xie and H. Yin, *Expert Opin. Ther. Pat.*, 2014, **24**, 131–154.
17 P. Wang, F. Yang, H. Yang, X. Xu, D. Liu, W. Xue and F. Zhu, *Bio-Med. Mater. Eng.*, 2015, **26**(suppl 1), S2233–S2239.
18 J. Prins, B. Olivier and S. M. Korte, *Expert Opin. Invest. Drugs*, 2011, **20**, 1107–1130.
19 E. J. Nestler and W. A. Carlezon, Jr., *Biol. Psychiatry*, 2006, **59**, 1151–1159.
20 L. Tao, F. Zhu, C. Qin, C. Zhang, F. Xu, C. Y. Tan, Y. Y. Jiang and Y. Z. Chen, *Nat. Biotechnol.*, 2014, **32**, 979–980.
21 H. Sharma, S. Santra and A. Dutta, *Future Med. Chem.*, 2015, **7**, 2385–2406.
22 S. Liu, C. Zha, K. Nacro, M. Hu, W. Cui, Y. L. Yang, U. Bhatt, A. Sambandam, M. Isherwood, L. Yet, M. T. Herr, S. Ebeltoft, C. Hassler, L. Fleming, A. D. Pechulis,

A. Payen-Fornicola, N. Holman, D. Milanowski, I. Cotterill, V. Mozhaev, Y. Khmelnitsky, P. R. Guzzo, B. J. Sargent, B. F. Molino, R. Olson, D. King, S. Lelas, Y. W. Li, K. Johnson, T. Molski, A. Orie, A. Ng, R. Haskell, W. Clarke, R. Bertekap, J. O'Connell, N. Lodge, M. Sinz, S. Adams, R. Zaczek and J. E. Macor, *ACS Med. Chem. Lett.*, 2014, **5**, 760–765.

23 F. Zhu, Z. Shi, C. Qin, L. Tao, X. Liu, F. Xu, L. Zhang, Y. Song, X. Liu, J. Zhang, B. Han, P. Zhang and Y. Chen, *Nucleic Acids Res.*, 2012, **40**, D1128–1136.

24 M. A. M. Subbaiah, *J. Med. Chem.*, 2017, DOI: 10.1021/acs.jmedchem.6b01827.

25 R. M. Lane, *J. Psychopharmacol.*, 2015, **29**, 526–544.

26 L. L. Miller, M. D. Leitl, M. L. Banks, B. E. Blough and S. S. Negus, *Pain*, 2015, **156**, 175–184.

27 E. D. Levin, C. Wells, J. E. Johnson, A. H. Rezvani, F. P. Bymaster and J. E. Rose, *Eur. J. Pharmacol.*, 2015, **764**, 30–37.

28 F. Zhu, X. H. Ma, C. Qin, L. Tao, X. Liu, Z. Shi, C. L. Zhang, C. Y. Tan, Y. Z. Chen and Y. Y. Jiang, *PLoS One*, 2012, **7**, e39782.

29 F. Zhu, C. Qin, L. Tao, X. Liu, Z. Shi, X. Ma, J. Jia, Y. Tan, C. Cui, J. Lin, C. Tan, Y. Jiang and Y. Chen, *Proc. Natl. Acad. Sci. U. S. A.*, 2011, **108**, 12943–12948.

30 P. Skolnick, P. Popik, A. Janowsky, B. Beer and A. S. Lippa, *Eur. J. Pharmacol.*, 2003, **461**, 99–104.

31 T. Hou, W. Zhang, J. Wang and W. Wang, *Proteins*, 2009, **74**, 837–846.

32 A. Yamashita, S. K. Singh, T. Kawate, Y. Jin and E. Gouaux, *Nature*, 2005, **437**, 215–223.

33 A. Penmatsa, K. H. Wang and E. Gouaux, *Nature*, 2013, **503**, 85–90.

34 F. Zhu, B. Han, P. Kumar, X. Liu, X. Ma, X. Wei, L. Huang, Y. Guo, L. Han, C. Zheng and Y. Chen, *Nucleic Acids Res.*, 2010, **38**, D787–791.

35 J. Andersen, L. Olsen, K. B. Hansen, O. Taboureau, F. S. Jorgensen, A. M. Jorgensen, B. Bang-Andersen, J. Egebjerg, K. Stromgaard and A. S. Kristensen, *J. Biol. Chem.*, 2010, **285**, 2051–2063.

36 J. Andersen, O. Taboureau, K. B. Hansen, L. Olsen, J. Egebjerg, K. Stromgaard and A. S. Kristensen, *J. Biol. Chem.*, 2009, **284**, 10276–10284.

37 H. Koldso, K. Severinsen, T. T. Tran, L. Celik, H. H. Jensen, O. Wiborg, B. Schiott and S. Sinning, *J. Am. Chem. Soc.*, 2010, **132**, 1311–1322.

38 J. Andersen, N. Stuhr-Hansen, L. G. Zachariassen, H. Koldso, B. Schiott, K. Stromgaard and A. S. Kristensen, *Mol. Pharmacol.*, 2014, **85**, 703–714.

39 W. Xue, P. Wang, B. Li, Y. Li, X. Xu, F. Yang, X. Yao, Y. Z. Chen, F. Xu and F. Zhu, *Phys. Chem. Chem. Phys.*, 2016, **18**, 3260–3271.

40 G. Zheng, W. Xue, P. Wang, F. Yang, B. Li, X. Li, Y. Li, X. Yao and F. Zhu, *Sci. Rep.*, 2016, **6**, 26883.

41 J. Grouleff, L. K. Ladefoged, H. Koldso and B. Schiott, *Front. Pharmacol.*, 2015, **6**, 235.

42 F. Zhu, L. Han, C. Zheng, B. Xie, M. T. Tammi, S. Yang, Y. Wei and Y. Chen, *J. Pharmacol. Exp. Ther.*, 2009, **330**, 304–315.

43 A. Anighoro, J. Bajorath and G. Rastelli, *J. Med. Chem.*, 2014, **57**, 7874–7887.

44 A. Lavecchia and C. Cerchia, *Drug Discovery Today*, 2016, **21**, 288–298.

45 W. Zhang, J. Pei and L. Lai, *J. Chem. Inf. Model.*, 2017, **57**, 403–412.

46 F. Zhu, C. J. Zheng, L. Y. Han, B. Xie, J. Jia, X. Liu, M. T. Tammi, S. Y. Yang, Y. Q. Wei and Y. Z. Chen, *Curr. Mol. Pharmacol.*, 2008, **1**, 213–232.

47 F. Zhu, L. Y. Han, X. Chen, H. H. Lin, S. Ong, B. Xie, H. L. Zhang and Y. Z. Chen, *Curr. Protein Pept. Sci.*, 2008, **9**, 70–95.

48 J. A. Coleman, E. M. Green and E. Gouaux, *Nature*, 2016, **532**, 334–339.

49 F. Yang, T. Fu, X. Zhang, J. Hu, W. Xue, G. Zheng, B. Li, Y. Li, X. Yao and F. Zhu, *Mol. Simul.*, 2017, **43**, 1089–1098.

50 K. H. Wang, A. Penmatsa and E. Gouaux, *Nature*, 2015, **521**, 322–327.

51 K. Arnold, L. Bordoli, J. Kopp and T. Schwede, *Bioinformatics*, 2006, **22**, 195–201.

52 M. A. Larkin, G. Blackshields, N. P. Brown, R. Chenna, P. A. McGettigan, H. McWilliam, F. Valentin, I. M. Wallace, A. Wilm, R. Lopez, J. D. Thompson, T. J. Gibson and D. G. Higgins, *Bioinformatics*, 2007, **23**, 2947–2948.

53 R. A. Laskowski, M. W. MacArthur, D. S. Moss and J. M. Thornton, *J. Appl. Crystallogr.*, 1993, **26**, 283–291.

54 PyMOL Molecular Graphics System v. 1.3, Schrödinger, LLC.

55 Glide v. 5.5, Schrödinger, LLC, New York, NY, 2009.

56 LigPrep v. 2.3, Schrödinger, LLC, New York, NY, 2009.

57 Epik v. 2.0, Schrödinger, LLC, New York, NY, 2009.

58 Maestro v. 9.0, Schrödinger, LLC, New York, NY, 2009.

59 L. Sorensen, J. Andersen, M. Thomsen, S. M. Hansen, X. Zhao, A. Sandelin, K. Stromgaard and A. S. Kristensen, *J. Biol. Chem.*, 2012, **287**, 43694–43707.

60 M. A. Lomize, I. D. Pogozheva, H. Joo, H. I. Mosberg and A. L. Lomize, *Nucleic Acids Res.*, 2012, **40**, D370–376.

61 E. L. Wu, X. Cheng, S. Jo, H. Rui, K. C. Song, E. M. Davila-Contreras, Y. Qi, J. Lee, V. Monje-Galvan, R. M. Venable, J. B. Klauda and W. Im, *J. Comput. Chem.*, 2014, **35**, 1997–2004.

62 V. Hornak, R. Abel, A. Okur, B. Strockbine, A. Roitberg and C. Simmerling, *Proteins*, 2006, **65**, 712–725.

63 AMBER v. 14, University of California, San Francisco, 2014.

64 C. J. Dickson, B. D. Madej, A. A. Skjevik, R. M. Betz, K. Teigen, I. R. Gould and R. C. Walker, *J. Chem. Theory Comput.*, 2014, **10**, 865–879.

65 I. S. Joung and T. E. Cheatham, 3rd, *J. Phys. Chem. B*, 2008, **112**, 9020–9041.

66 C. I. Bayly, P. Cieplak, W. Cornell and P. A. Kollman, *J. Phys. Chem.*, 1993, **97**, 10269–10280.

67 Gaussian 09 v. D.01, Gaussian, Inc., Wallingford CT, 2009.

68 T. Darden, D. York and L. Pedersen, *J. Phys. Chem.*, 1993, **98**, 10089–10092.

69 M. Springborg and B. Kirtman, *J. Phys. Chem.*, 2007, **126**, 104107.

70 P. A. Kollman, I. Massova, C. Reyes, B. Kuhn, S. Huo, L. Chong, M. Lee, T. Lee, Y. Duan, W. Wang, O. Donini,

P. Cieplak, J. Srinivasan, D. A. Case and T. E. Cheatham, 3rd, *Acc. Chem. Res.*, 2000, **33**, 889–897.
71 I. Massova and P. A. Kollman, *Perspect. Drug Discovery Des.*, 2000, **18**, 113–135.
72 B. Li, J. Tang, Q. Yang, X. Cui, S. Li, S. Chen, Q. Cao, W. Xue, N. Chen and F. Zhu, *Sci. Rep.*, 2016, **6**, 38881.
73 J. Wang, P. Morin, W. Wang and P. A. Kollman, *J. Am. Chem. Soc.*, 2001, **123**, 5221–5230.
74 A. Onufriev, D. Bashford and D. A. Case, *Proteins*, 2004, **55**, 383–394.
75 G. G. Froesner, D. A. Peterson, F. W. Deinhardt and A. W. Holmes, *Lancet*, 1973, **1**, 1183.
76 M. L. Connolly, *J. Appl. Crystallogr.*, 1983, **16**, 548–558.
77 S. Tippmann, *Nature*, 2015, **517**, 109–110.
78 M. R. Barer and C. R. Harwood, *Adv. Microb. Physiol.*, 1999, **41**, 93–137.
79 I. Letunic and P. Bork, *Bioinformatics*, 2007, **23**, 127–128.
80 D. C. Deecher, C. E. Beyer, G. Johnston, J. Bray, S. Shah, M. Abou-Gharbia and T. H. Andree, *J. Pharmacol. Exp. Ther.*, 2006, **318**, 657–665.
81 L. Xu, H. Sun, Y. Li, J. Wang and T. Hou, *J. Phys. Chem. B*, 2013, **117**, 8408–8421.
82 M. Aldeghi, A. Heifetz, M. J. Bodkin, S. Knapp and P. C. Biggin, *Chem. Sci.*, 2016, **7**, 207–218.
83 W. L. Jorgensen and L. L. Thomas, *J. Chem. Theory Comput.*, 2008, **4**, 869–876.
84 G. Rastelli, A. Del Rio, G. Degliesposti and M. Sgobba, *J. Comput. Chem.*, 2010, **31**, 797–810.
85 H. Sun, Y. Li, S. Tian, L. Xu and T. Hou, *Phys. Chem. Chem. Phys.*, 2014, **16**, 16719–16729.
86 F. Chen, H. Liu, H. Sun, P. Pan, Y. Li, D. Li and T. Hou, *Phys. Chem. Chem. Phys.*, 2016, **18**, 22129–22139.
87 G. Palermo, A. D. Favia, M. Convertino and M. De Vivo, *ChemMedChem*, 2016, **11**, 1252–1258.
88 P. Wang, T. Fu, X. Zhang, F. Yang, G. Zheng, W. Xue, Y. Chen, X. Yao and F. Zhu, *Biochim. Biophys. Acta*, 2017, **1861**, 2766–2777.
89 W. Xue, F. Yang, P. Wang, G. Zheng, Y. Chen, X. Yao and F. Zhu, *ACS Chem. Neurosci.*, 2018, DOI: 10.1021/acschemneuro.7b00490.
90 B. Li, J. Tang, Q. Yang, S. Li, X. Cui, Y. Li, Y. Chen, W. Xue, X. Li and F. Zhu, *Nucleic Acids Res.*, 2017, **45**, W162–W170.
91 S. Genheden and U. Ryde, *Expert Opin. Drug Discovery*, 2015, **10**, 449–461.
92 T. Hou, J. Wang, Y. Li and W. Wang, *J. Chem. Inf. Model.*, 2011, **51**, 69–82.
93 C. M. Reyes and P. A. Kollman, *J. Mol. Biol.*, 2000, **297**, 1145–1158.
94 C. Y. Yu, X. X. Li, H. Yang, Y. H. Li, W. W. Xue, Y. Z. Chen, L. Tao and F. Zhu, *Int. J. Mol. Sci.*, 2018, 19.
95 C. Zhang, L. Tao, C. Qin, P. Zhang, S. Chen, X. Zeng, F. Xu, Z. Chen, S. Y. Yang and Y. Z. Chen, *Nucleic Acids Res.*, 2015, **43**, D558–565.
96 L. M. Espinoza-Fonseca, *Bioorg. Med. Chem.*, 2006, **14**, 896–897.

